Supporting Information

Conductive Co-triazole metal-organic framework exploited as oxygen evolution electrocatalyst

Kanyaporn Adpakpang,[a] Ladawan Pukdeejorhor,[a] Lappawat Ngamwongwan,[b] Suwit Suthirakun,[c] Sarawoot Impeng,[d] Suttipong Wannapaiboon,[e] Pongkarn Chakthranont,[d] Kajornsak Faungnawakij,[d] and Sareeya Bureekaew*[a]

[a.] School of Energy Science and Engineering, Vidyasirimedhi Institute of Science and Technology, 555 Moo 1 Payupnai, Wangchan, Rayong 21210, Thailand.

[b.] School of Physics, Institute of Science, Suranaree University of Technology, Nakhon Ratchasima 30000, Thailand

[c.] School of Chemistry, Institute of Science, Suranaree University of Technology, Nakhon Ratchasima 30000, Thailand.

[d.] National Nanotechnology Center (NANOTEC), National Science and Technology Development Agency (NSTDA), 111 Thailand Science Park, Pahonyothin Rd., Klong Laung, Pathum Thani 12120, Thailand.

[e.] Synchrotron Light Research Institute, 111 University Avenue, Muang, Nakhon Ratchasima 30000, Thailand.

Synthesis of Co-trz MOF

Co-trz, [Co_2(triazole)$_3$Cl], was synthesized via microwave method. First, 1.6 mmol of $CoCl_2 \cdot 6H_2O$ (Sigma Aldrich, >99%) and 3.4 mmol of 1,2,4-triazole (TCI, 98%) were mixed in 10 g of deionized water in 35 mL-microwave vial and stirred at room temperature to obtain a homogeneous solution. Then, the vial was transferred to a microwave heating chamber (CEM discover SP) and heated to 160 ^oC for 10 min, obtaining the purple product. After cooling down, the obtained precipitates were separated out by centrifugation at 14000 rpm. The collected solid was washed with DI water and ethanol and dried in vacuum oven at 50 ^oC prior to use.

Material Characterization

Crystal phase identification was performed using powder X-ray diffractometer (PXRD, Bruker, New D8 advance, Cu Kα, λ = 1.5406 Å). Product morphology and elemental analyses were examined by using a field-emission scanning electron microscope (FE-SEM, JEOL, JSM-7610F) equipped with energy dispersive spectroscopy (EDS, Oxford X-max 150 mm^2) operating in gentle beam mode (0.5-2.0 kV). Before measurement, the samples were spluttered with platinum at 10 mA for 30 sec to increase the surface conductivity. Morphological study with phase analysis was performed by using transmission electron microscopy operated at 200 kV (TEM, JEOL, JEM-ARM 200F). STEM-EDS was applied for elemental distribution (Digiscan, Gatan). Nitrogen adsorption experiment was done at 77 K using BELMAX (Japan). The sample was evacuated at 120 ^oC before measurement. Thermogravimetric analysis (TGA) was performed under N_2 atmosphere with the ramping rate of 10 ^oC min^{-1} using ThermoPlus EVO2 (Rigaku, Japan). Mechanistic study of electrochemical reaction pathway was characterized by synchrotron-based X-ray absorption near edge structure (XANES) and extended X-ray absorption fine structure (EXAFS) of Co K-edge. Working electrodes for mechanistic study were prepared by dropping the prepared catalyst ink onto conductive carbon film with controlled the loading of 0.28 mg cm^{-2} on 5 mm diameter area. After letting dry, the electrodes were electrochemically examined both in linear-sweep voltammetry and chronoamperometry modes. After the experiment, the as-prepared and tested electrodes were immediately kept closed by attaching Kapton tape on both sides in order to avoid any other unwanted factors. The experiments were performed at beamline BL1.1W: Multiple X-ray Techniques Beamline, Synchrotron Light Research Institute, Thailand. The measurement was conducted at ambient temperature and pressure by simultaneously measuring the samples together with the Co foils as a standard reference for an in-line alignment of the energy shift during the synchrotron operation. The obtained data were

analyzed using ATHENA analysis package. Fourier-transform in the k-range of 3.0-10.0 Å (k^3-weighing) was performed. The obtained FT-amplitude plots were compared.

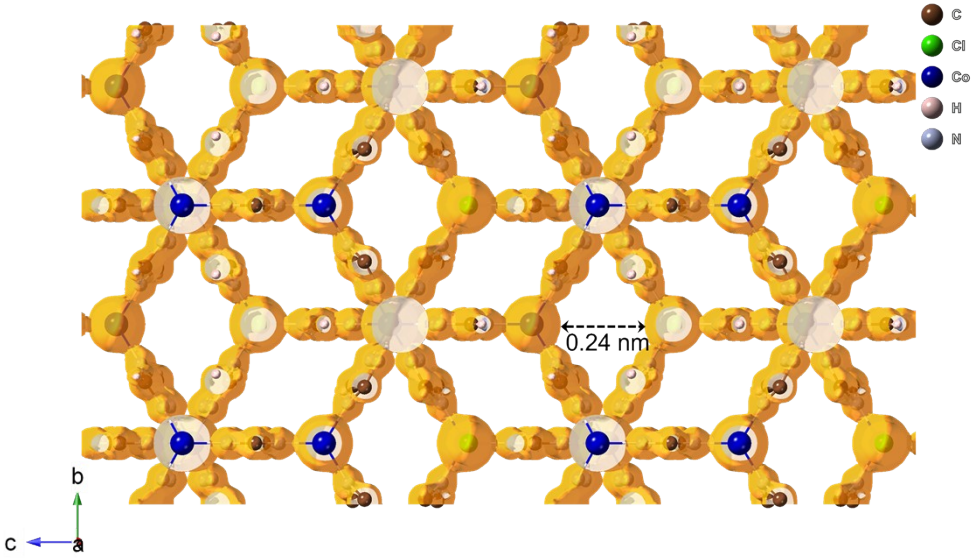

Fig. S1 Crystal structure of Co-MOF viewed along a-axis.[1]

: Along a-axis, Co-MOF provided pore channel with a diameter of 0.24 nm which was accessible for transport of hydroxide ions and evolved oxygen associated in oxygen evolution reaction.

Computational details

All calculations reported herein were carried out using spin-polarized density functional theory (DFT) as implemented in the Vienna Ab-initio Simulation Package (VASP)[2-4]. The exchange and correlation functional was approximated using the Perdew–Burke–Ernzerhof functional[5] with dispersion correction of PBE-D3[6] as it accurately predicts lattice constants of various MOF systems.[7,8] We chose the ultra-soft pseudopotential with projector augmented-wave (PAW) method[9,10] to describe the interactions between frozen cores and valence electrons. The valence electron wave functions were represented in a plane-wave basis with a kinetic energy cut-off of 500 eV. The orthorhombic unit cell of Co-trz MOF containing 96 atoms was taken. (Fig. S2). A Gaussian smearing (Sigma = 0.05 eV) was used during geometry optimization in which the calculated energies were extrapolated to zero smearing width. The ion positions were optimized using the Monkhorst-Pack approach[11] with a k-point sampling of 7 × 5 × 3. The optimized structure was attained when the calculated residual forces were less than 0.01 eV/Å. Two Co centers are distinguished including six-fold octahedral Co1 and four-fold tetrahedral Co2 centers, as shown in Fig. S2. Three possible magnetic configurations of the Co centers including ferromagnetic (FM), antiferromagnetic (AFM) and competing antiferromagnetic (c-AFM) configurations were considerably investigated. The FM configuration exhibits paralleled spins for all Co centers whereas the AFM configuration includes anti-parallelly aligned among the Co1 spins and the Co2 spins themselves yielding a net zero magnetic moment. The c-AFM configuration corresponds to the Co1 spins anti-parallelly aligned with the Co2 spins where these spins were not completely cancelled out resulting in a non-zero magnetic moment. The calculations revealed that the c-AFM is the most stable configuration which was 0.75 eV and 0.31 eV more stable in energy than those of the FM and AFM configurations, respectively. The c-AFM configuration resulted in competing magnetic moments of -0.63 μB for Co1 centers and +2.31 μB for Co2 centers, suggesting a weak ferromagneticity at low temperature. The calculated results agreed with previous experimental observations that the Co-trz exhibited competing antiferromagnetic behavior.[1]

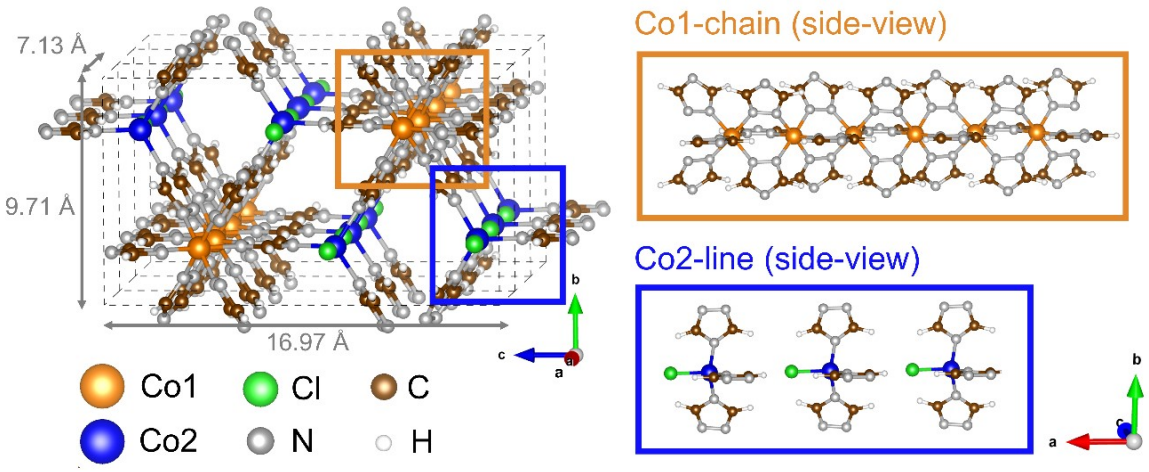

Fig. S2 Periodic structure of Co-trz MOF. Color codes; Co1: orange, Co2: blue, Cl: green, N: grey, C: brown, H white.

Electrocatalytic activity testing condition

Catalyst ink was prepared by dispersing 5 mg of Co-trz in DI water (0.8 mL) and isopropanol (0.2 mL) with an addition of 20 µL Nafion (Sigma-Aldrich, 5 %wt. in water-alcohol mixture). The homogeneous dispersion of catalyst inks was promoted by ultrasonication. 4 uL of the prepared ink was dropped onto glassy carbon rotating disk electrode (GE-RDE, 3 mm di, ALS Japan) and dried in an oven. The catalyst loading was 0.28 mg cm^{-2}. For comparison, catalyst ink of commercial IrO_2 (Alfa-Aesar, electronic grade, 99.99%) was prepared in the similar manner. The obtained dried working electrode was subsequently tested for oxygen evolution reaction (OER) in oxygen-saturated potassium hydroxide (1 M KOH, pH14) aqueous electrolyte using platinum rod and Hg/HgO electrode (1 M NaOH filled electrolyte) as counter and reference electrodes, respectively. The test was performed at rotating speed of 1,600 rpm on an electrochemical working station (RRDE-3A, ALS Japan) and examined with a potentiostat (Palmsens 4, Netherlands). OER polarization curves were collected in linear-sweep voltammetry (LSV) mode scanning from 0.1-0.85 V (vs. Hg/HgO) with scan rate of 5 mV sec^{-1}. Before collecting LSV curves, the Co-trz working electrode was activated by cyclic voltammetry (CV) scan between 0.1-0.85 V (vs. Hg/HgO) at scan rate of 50 mV sec^{-1}. The activation process was ensured when obtaining the steady polarization curve. OER overpotential (η) was obtained by a subtraction of theoretical thermodynamic potential (1.23 V vs. RHE) from the observed potentials. Reaction kinetics was analyzed based on the Tafel slopes acquired from the Tafel plots according to equation (1) which η, a, b, and j were overpotential, Tafel constant, Tafel slope and current density, respectively.

$$\eta = a + b \log j \qquad \text{(Eq. 1)}$$

Reference electrode potential calibration

To obtain an exact potential value of Hg/HgO electrode used as reference electrode for electrocatalyst test, the electrode was calibrated in a three-electrode system using Pt wires as working electrode and counter electrode. The experiment was carried out in H_2-saturated 1 M KOH electrolyte. Prior to the measurement, the electrolyte was saturated with high-purity hydrogen for 30 min. Then, CV test was performed. As depicted in Fig. S3, an average number at the zero-current points was determined to be -0.928 V. Therefore, the experimentally obtained potential can be converted to reversible hydrogen electrode (RHE) scale as E (V vs. RHE) = E (V vs. Hg/HgO) + 0.928 V.[12] The measured value was close to the theoretical one (0.924 V) calculated based on the measured pH value (14.00).

Theoretical value calculation: $E\ (V\ vs.\ RHE) = E\ (V\ vs.\ Hg/HgO) + E^{0}_{Hg/HgO} + (0.059 \times pH)$

$= E\ (V\ vs.\ Hg/HgO) + 0.098 + (0.059 \times 14.00)$

$= E\ (V\ vs.\ Hg/HgO) + 0.924\ V$ (Eq. 2)

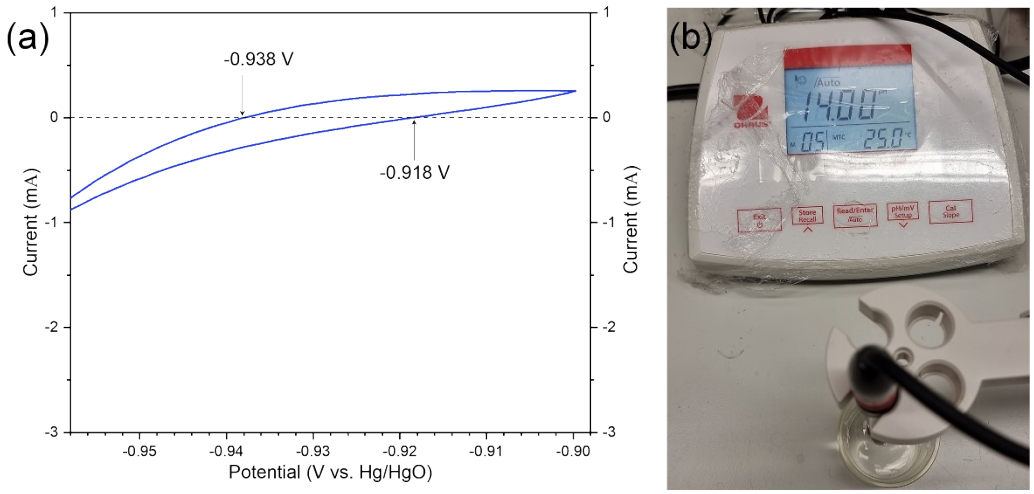

Fig. S3 (a) Reference electrode calibration and (b) pH measurement at 25 °C.

Electrochemical impedance spectroscopy (EIS) measurement and iR compensation

Electrochemical impedance spectroscopy (EIS) was performed at the applied ac amplitude of 5 mV with the frequency ranging from 0.01-100 kHz. EIS plots and fitting results were presented in Fig. S4 and Table S1.

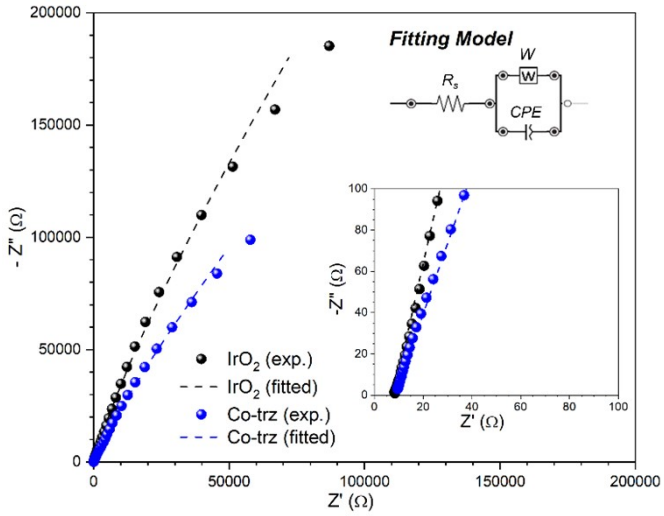

Fig. S4 Nyquist plots of Co-trz as compared to IrO_2 with (insets) the expanded view and fitted model.

Table S1 EIS fitted data of Co-trz electrode as compared to IrO_2.

Sample	Electrolyte resistance (R_s) / Ω		Warburg element (W) / kσ		Constant phase element (CPE) / μT	
	Fitted value	% Error	Fitted value	% Error	Fitted value	% Error
Co-trz	8.31	0.69	36.23	13.09	50.66	1.28
IrO_2	8.50	0.75	97.44	5.94	41.43	1.22

According to the EIS results, both the Co-trz and IrO_2 working electrodes possessed the electrolyte resistance about 8 Ω. The obtained resistance was employed to compensate an iR-drop of the experimentally obtained potential for 90% (90% iR-compensation). The compensated potential was acquired based on equation (3) and reported throughout the work unless specify.

$$E = E_{experimetal} - iR \qquad \text{(Eq. 3)}$$

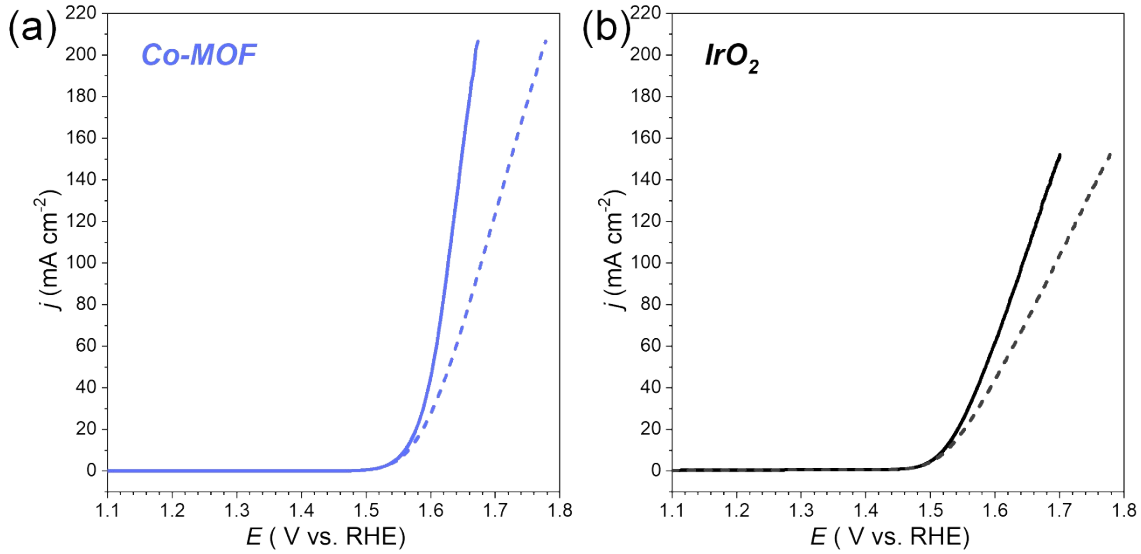

Fig. S5 Polarization curves of (a) Co-MOF and (b) IrO_2. Solid and dashed lines represent the data with and without 90% iR-compensation, respectively.

Evaluation of Faradaic efficiency (FE)[13-15]

Faradaic efficiency of Co-MOF catalyst was evaluated using rotating ring-disk electrode (RRDE) method. Glassy carbon disk (4 mm diameter) with Pt-ring (7 mm/5 mm for outer/inner diameter) RRDE was purchased from ALS, Japan. Through this method, upon the positive potential sweep, oxygen gas from OER generated on the catalyst coated GC-disk electrode surface will be collected and reduced on Pt-ring electrode with applied potential for applicable ORR (E_{ring}=0.4 V vs. RHE) as depicted in Fig. S6. An efficiency of electron-transfer that was related to the production of oxygen namely Faradaic efficiency (FE) can be then derived from the observed current at ring electrode (I_{ring}) to current at disk electrode (I_{disk}) with a collection efficiency (N) of specific type of electrode, FE (%) = $I_{ring}/(I_{disk} \times N)$.

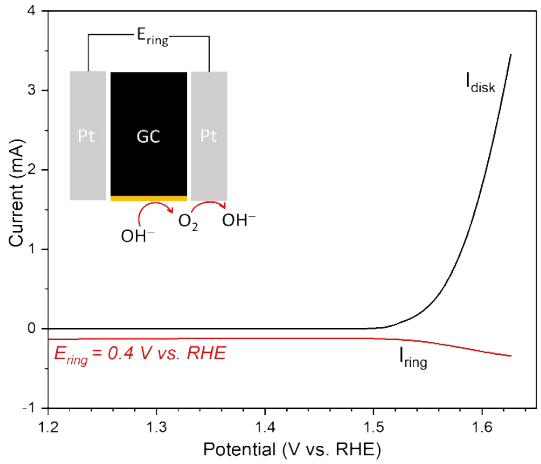

Fig. S6 LSV curves of Co-MOF on GCE with an applied ring potential of 0.4 V vs. RHE. Reaction performed in N_2-saturated 1 M KOH electrolyte with the RRDE rotation speed of 1600 rpm. Potential presented without iR-correction.

To gain an information on N value, the polished RRDE electrode was employed in an experiment of ferrocyanide/ferricyanide half reaction. The reaction was performed in 10 mM $K_3[Fe(CN)_6]_6$ in N_2-saturated solution of 1 M KNO_3 at the scan rate of 1600 rpm. Potential of disk electrode was scanned from 0.4 V to -0.4 V vs. Ag/AgCl with the applied ring potential of 0.6 V vs. Ag/AgCl. N value was calculated to be 0.4. This obtained value was exploited for the calculation of FE at various numbers of overpotential through chronoamperometry method. Towards each applied disk potentials, the ring potential was fixed at 0.4 V vs. RHE. The resulting I_{ring} and I_{disk} were used for FE as shown in Fig. S7.

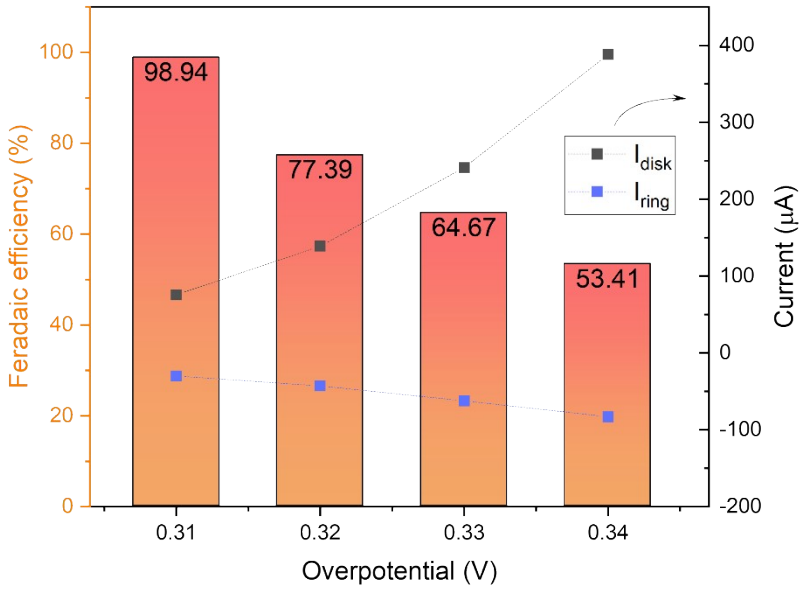

Fig. S7 Faradaic efficiency of Co-trz at various overpotentials.

Calculation of mass activity (MA)

Mass activity (A g^{-1}) at each considered overpotential was determined by dividing its current density (mA cm^{-2}) with the mass of electrocatalyst loaded on the electrode (mg cm^{-2}).

Determination of turnover frequency (TOF)

Turnover frequency was evaluated by assuming that tetrahedral Co site acted as active site based on the following equation.

$$TOF = j \times A / (4 \times F \times n_{Co})$$

Where, j = observed current density at the considered overpotential (mA cm^{-2})

A = geometrical surface area (0.0707 cm^2)

F = faraday constant (96485 C mol^{-1})

n_{Co} = number of Co active sites (mol)

In this study, we considered that tetrahedral Co (Co_{tet}), half amount of the overall Co, was responsible for active site. n_{Co} was therefore calculated as follow.

n_{Co} = (weight(%) of Co_{tet} in Co-MOF x catalyst loading x loaded volume) / atomic mass of Co

According to the calculation by 16.25 %wt. of Co_{tet} resided in Co-MOF, TOF of Co-MOF catalyst at various overpotential can be obtained.

Electrochemical active surface area (ECSA) determination

CV test in non-faradaic region (1.08 – 1.28 V vs. RHE) was performed on Co-MOF catalyst loaded on glassy carbon in the similar manner with the catalytic testing condition. The CV measurement was carried out at the scan rates of 10, 20, 40, 60, and 80 mV s^{-1} (Fig. S8a). From CV curves, the average of capacitive current densities ($\Delta j/2$), $\Delta j=|j_a-j_c|$ at 1.18 V vs. RHE from all the applied scan rates were plotted as a function of the scan rates (Fig. S8b). Double-layer capacitance (C_{dl}) of the electrode can be obtained from linear slope of the plot which was 0.319 mF cm^{-2}. From the obtained $C_{dl,}$ ECSA can be determined from C_{dl}/C_s where Cs is capacitive behavior typical known as 0.04 mF cm^{-2} per cm_{ECSA}^2 for the flat surface electrode in 1.0 M KOH.[16,17] Therefore, ECSA of Co-MOF electrode was determined to be 7.98 cm^2 which was acceptable for this 1D-channel structure with limited pore size.

.

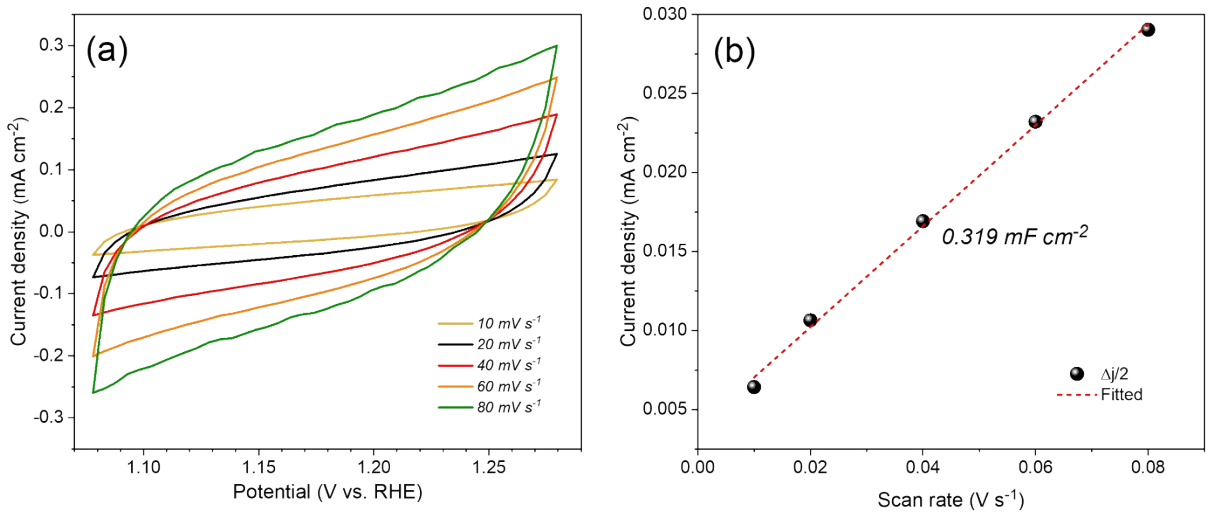

Fig. S8 (a) CV curves of Co-MOF and corresponded (b) $\Delta j/2$ at 1.18 V vs. RHE for various scan rates. Potential presented without iR-correction.

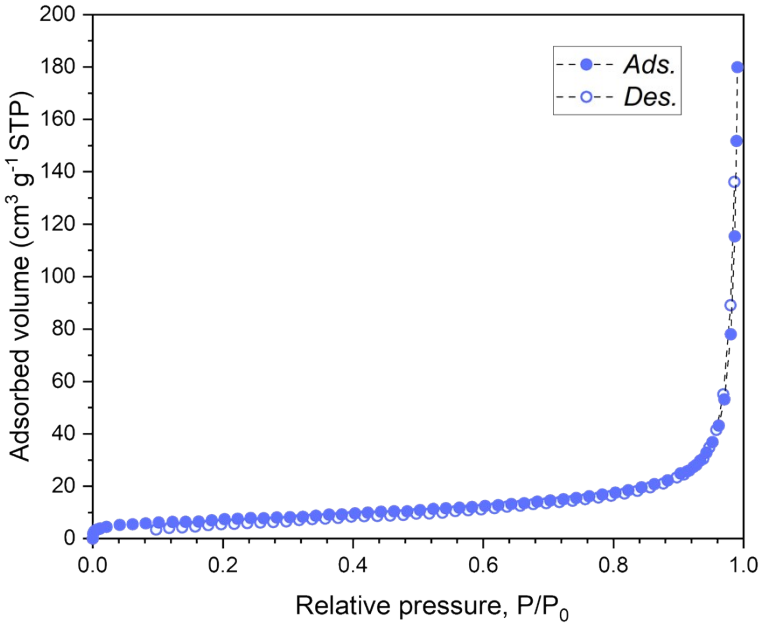

Fig. S9 N_2 adsorption isotherm of Co-MOF at 77 K.

: N_2 adsorption isotherm of Co-MOF is classified to Type II for non-porous materials. This is ascribable for the limited accessible size of the framework for N_2 gas. Specific surface area calculated based on Brunauer–Emmett–Teller (BET) method (S_{BET}) was 25 m^2 g^{-1}. TGA result of Co-MOF indicated its limited pore volume (Fig. S11).

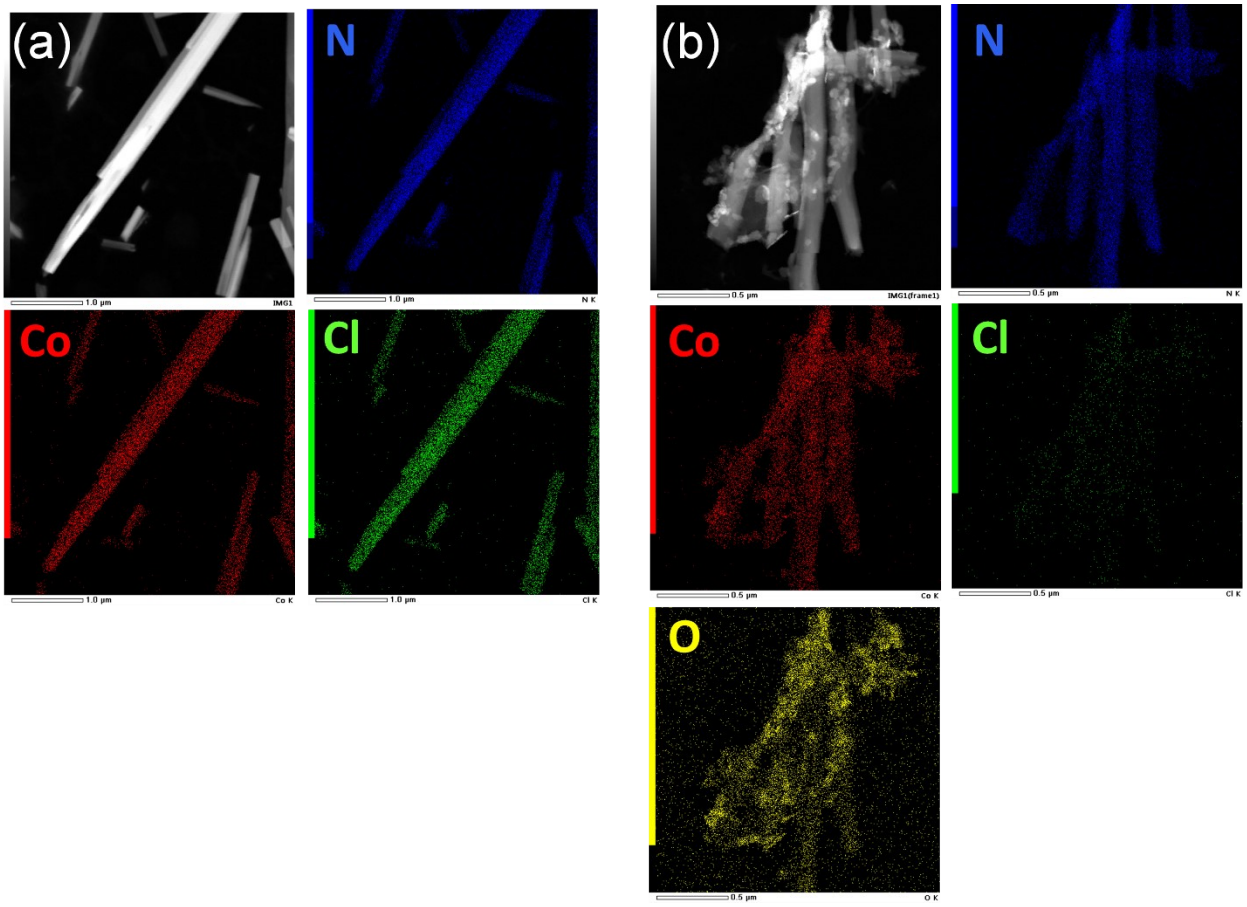

Fig. S10 STEM-EDS mapping of Co-trz (a) before and (b) after chronoamperometry at η_{10} for 10 h.

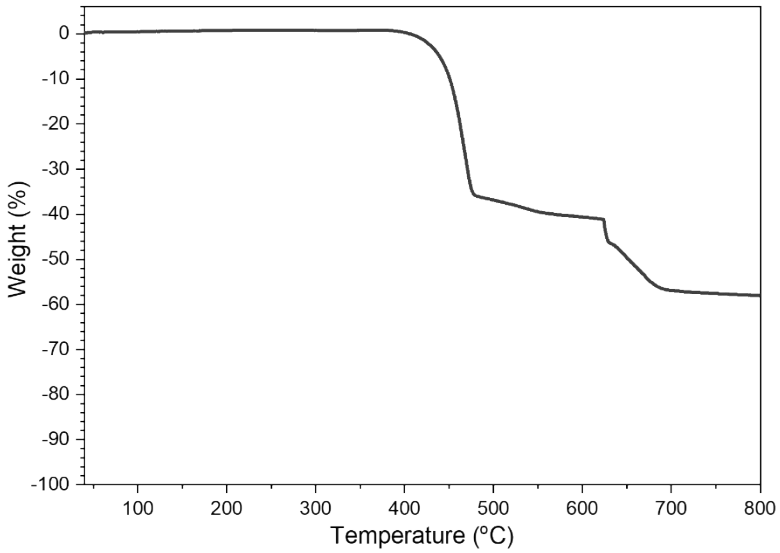

Fig. S11 TGA plot of the synthesized Co-trz MOF.

: TGA profile showed that the Co-MOF product was thermally stable up to ~450 °C. The result exhibited no weight loss regarding to the removal of solvent in the pore, suggesting its limited pore volume.

Table S2 OER performance of Co-based catalysts as compared to Co-MOF in this study.

Catalyst	η_{10} (mV)	Tafel slope (mV dec^{-1})	Electrolyte	TOF (s^{-1}) at 400 mV	Ref.
Co-trz MOF	330	55	1.0 M KOH	*6.6	This work
2D flake Co-BDC	410	83	1.0 M KOH	-	S18
Co2-tzpa	336	58	1.0 M KOH	-	S19
Co-BDC	334	-	1.0 M KOH	-	S20
Co-ZIF-67	341	-	1.0 M KOH	-	S20
2D Co-BPDC/Co-BDC-3 heterojunction	335	72	1.0 M KOH	-	S21
Co-MOF/NF	311 (η50)	77	1.0 M KOH	0.18	S22
Co-MOF powder on NF	362 (η50)	89	1.0 M KOH	-	S22
Co-MOF NS	263	74	1.0 M KOH	0.4	S23
Micro-nano Co-MOF	287	94	1.0 M KOH	-	S23
Bulk Co-MOF	326	122	1.0 M KOH	-	S23
Co_2(benzimidazole)$_4$	348	-	1.0 M KOH	-	S24
$Co_3(\mu_3\text{-OH})(COO)_6$	540	-	1.0 M NaOH	-	S25

*Calculated based on tetrahedral Co site, responsible for catalytic center. TOF was 3.3 s^{-1} for overall Co species in Co-trz.

References

S1. W. Ouellette, J. R. Galán-Mascarós, Kim R. Dunbar and J. Zubieta, *Inorg. Chem*., 2006, **45**, 1909-1911.

S2. G. Kresse, J. Hafner, *Phys. Rev. B,* 1993, **47**, 558-561.

S3. G. Kresse, J. Furthmüller, *Comput. Mater. Sci.,* 1996, **6**, 15-50.

S4. G. Kresse, J. Furthmüller*, Phys. Rev. B,* 1996, **54**, 11169-11186.

S5. J. P. Perdew, K. Burke, M. Ernzerhof, *Phys. Rev. Lett.,* 1996, **77**, 3865-3868.

S6. S. Grimme, J. Antony, S. Ehrlich, H. Krieg, *J. Chem. Phys.,* 2010, **132**, 154104.

S7. D. Nazarian, P. Ganesh, D. S. Sholl, *J. Mater. Chem. A,* 2015, **3**, 22432-22440.

S8. A. S. Rosen, M. R. Mian, T. Islamoglu, H. Chen, O. K. Farha, J. M. Notestein, R. Q. Snurr, *J. Am. Chem. Soc.,* 2020, **142**, 4317-4328.

S9. G. Kresse, D. Joubert, *Phys. Rev. B,* 1999, **59**, 1758-1775.

S10. P. E. Blöchl, *Phys. Rev. B,* 1994, **50**, 17953-17979.

S11. H. J. Monkhorst, J. D. Pack, *Phys. Rev. B,* 1976, **13**, 5188-5192.

S12 S. Niu, S. Li, Y. Du, X. Han, P. Xu, *ACS Energy Lett.*, 2020, **5**, 1083–1087.

S13 B. Mohanty, Y. Wei, M. Ghorbani-Asl, A. V. Krasheninnikov, P. Rajpute, B. K. Jena, *J. Mater. Chem. A,* 2020, **8**, 6709-6716.

S14 S. Zhao, Y. Wang, J. Dong, C.-T. He, H. Yin, P. An, K. Zhao, X. Zhang, C. Gao, L. Zhang, J. Lv, J. Wang, J. Zhang, A. M. Khattak, N. A. Khan, Z. Wei, J. Zhang, S. Liu, H. Zhao, Z. Tang, *Nat. Energy,* 2016, **1**, 16184.

S15 J. Masud, A. T. Swesi, W. P. R. Liyanage, M. Nath, *ACS Appl. Mater. Interfaces,* 2016, **8**, 17292-17302.

S16 Y. Li, C. Zhao, *ACS Catal.,* 2017, **7**, 2535– 2541.

S17 Q. Q. Sun, Y. J. Dong, Z. L. Wang, S. W. Yin, C. Zhao, *Small,* 2018, **14**, 1704137.

S18 F. Li, J. Li, L. Zhou, S. Dai, *Sustain. Energy Fuels,* 2021, **5**, 1095-1102.

S19 N. Liu, Q. Zhang, J. Guan, *Chem. Commun*., 2021, **57**, 5016-5019.

S20 X. Cai, F. Peng, X. Luo, X. Ye, J. Zhou, X. Lang, M. Shi, *ChemSusChem,* 2021, **14**, 3163-3173.

S21 Q. Zha, F. Yuan, G. Qin, Y. Ni, *Inorg. Chem*., 2020, **59**, 1295–1305.

S22 X. Zhang, W. Sun, H. Du, R.-M. Kong, F. Qu, *Inorg. Chem. Front*., 2018, **5**, 344-347.

S23 Y. Xu, B. Li, S. Zheng, P. Wu, J. Zhan, H. Xue, Q. Xu, H. Pang, *J. Mater. Chem. A,* 2018, **6**, 22070-22076.

S24 W. Zhang, Y. Wang, H. Zheng, R. Li, Y. Tang, B. Li, C. Zhu, L. You, M. R. Gao, Z. Liu, S. H. Yu, K. Zhou, *ACS Nano,* 2020, **14**, 1971-1981.

S25 K. Nath, K. Bhunia, D. Pradhan, K. Biradha, *Nanoscale Adv*., 2019, **1**, 2293-2302.